[13] A. Alomainy, Y. Hao, and D. M. Davenport, "Parametric study of wearable antennas with varying distances from the body and different on-body positions," in *Proc. IET Seminar on Antennas and Propagation for Body-Centric Wireless Communications*, London, Apr. 2007, pp. 84–89.
[14] P. Salonen, L. Sydänheimo, M. Keskilammi, and M. Kivikoski, "A small planar inverted-F antenna for wearable applications," in *Proc. 3rd Int. Symp. on Wearable Computers*, San Diego, CA, Oct. 1999, pp. 95–100.
[15] HFSS 3D Full-Wave Electromagnetic Field Simulation for RF, Wireless, Packaging, and Optoelectronic Design Ansoft [Online]. Available: www.ansoft.com
[16] [Online]. Available: http://transition.fcc.gov/oet/rfsafety/dielectric.html

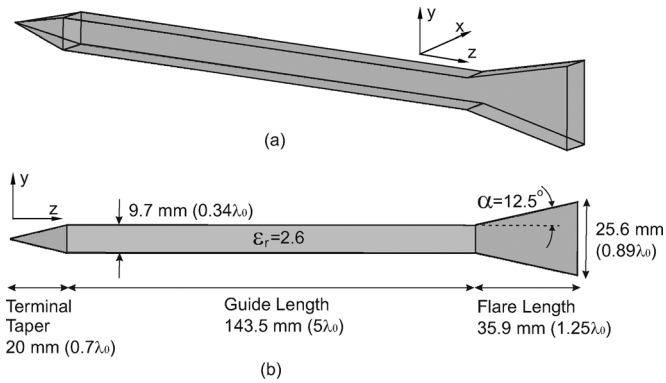

Fig. 1. Dielectric field enhancer dimensions.

Dielectric Field Enhancer for Reconfiguring the Beam Pattern and Gain of an Antenna

Philip W. C. Hon, Ali Ayazi, Bahram Jalali, and Tatsuo Itoh

***Abstract*—We demonstrate the use of a dielectric rod, herein called a dielectric field enhancer (DFE), to reconfigure the radiation pattern and gain of an omni-directional antenna. To assess the DFE capability, we demonstrate an increase in gain of a preexisting antenna by near-field coupling with the DFE. The resulting field pattern is observed to be a hybrid of the DFE's directive beam pattern and that of the preexisting antenna. Measurements of a prototype DFE show a gain increase of at least 7.7 dB after the inclusion of the DFE, which compare well with simulations and therefore verify the capability of the DFE.**

***Index Terms*—Dielectric resonator antenna, dielectric rod antenna, field enhancement, gain enhancement, reconfigurable antennas.**

I. Introduction

Wireless communication systems such as 3G, and 4G systems have driven the need for reconfigurable antennas, where the reconfigurability of an antenna could be its resonant frequency, polarization, beam pattern or any combination of the three [1]. Reconfigurability can be achieved in many different ways. One can use electromagnetic bandgap structures [2] or manipulate current paths by using switches or diodes [3].

In this communication, we present the characteristics of a modified dielectric rod antenna that acts as a passive field enhancer that can be used to reconfigure the radiation pattern and gain of an omni-directional antenna. Under near-field coupling conditions to a preexisting antenna, the dielectric field enhancer (DFE) reconfigures the radiation pattern and increases the gain of the overall system. Such a structure is desirable in applications that require gain improvement or highly localized fields such as in the all-dielectric non-electronic radio front-end system (ADNERF) [4], [5]. Indeed, other antennas such as long Yagi-Uda arrays, could provide similar gain improvements. However, the DFE's bandwidth is greater than the considerably more dispersive Yagi-Uda arrays and hence is a good candidate for applications with larger bandwidth requirements [6].

The design methodology for the DFE is detailed in Section II. Verification of the design is conducted with a preexisting annular ring dielectric resonator antenna (DRA) and is discussed in Section III. The objective is to verify the increase in the annular ring DRA's gain after the inclusion of the DFE, and hence the DFE's field enhancing capability. Measurement results compared with full-wave finite element method (Ansys' HFSS) simulations are presented.

Manuscript received November 15, 2011; revised March 07, 2012; accepted April 16, 2012. Date of publication July 03, 2012; date of current version August 30, 2012. This work was supported in part by the DARPA EMPiRe Program.

The authors are with the Department of Electrical Engineering, University of California, Los Angeles, CA 90095 USA (e-mail: phon@ee.ucla.edu).

Color versions of one or more of the figures in this communication are available online at http://ieeexplore.ieee.org.

Digital Object Identifier 10.1109/TAP.2012.2207067

II. Analysis and Design

The design of the DFE requires consideration of the far-field radiation pattern, as for a traditional dielectric rod antenna, as well as the near-field interaction with the excitor/feed antenna. Far-field gain is optimized by controlling the cross section, permittivity and length of the structure while the near-field consideration is done by controlling the coupling aperture section's (E-plane sectoral horn section) flare angle. The excited mode, TE_{11}^{x}, with reference to Fig. 1(a), in the DFE is well suited for coupling to and from an annular ring DRA that is resonating in its electric monopole $\mathrm{TM}_{010+\delta}$ mode. Efficient coupling is achieved due to the co-polarized near fields of the DFE and annular ring DRA.

A. Dielectric Field Enhancer

In a traditional dielectric rod antenna, the length of the guided region dictates the achievable gain of the antenna, as mentioned in [6], [7], for a given cross section and permittivity. The objective is to design a DFE, with a certain gain, that will provide the maximum achievable coupling to an annular ring DRA.

The DFE was designed in two steps. First, using the phase velocity versus cross sectional dimension design curves in [6], a rectangular cross section dielectric rod was designed. This portion of the design consisted of a free space to dielectric impedance transforming terminal taper and a waveguiding section. The above is done to insure a well coupled and guided mode in the dielectric rod. The terminal taper dimension of slightly greater than half a wavelength was found to be sufficient in our simulations for good coupling. As a starting point, an assumed gain of 16 dBi for a traditional rod antenna was made and the cross sectional dimensions were acquired from [6]. A cross-linked polystyrene is used for the dielectric with permittivity of 2.6, and a loss tangent of 0.0007. This results in a square cross-section having a side of 9.7 mm at 10.45 GHz. The length of the guided region based on the dielectric permittivity, desired gain and cross section comes out to be 143.5 mm $(5\lambda_0)$.

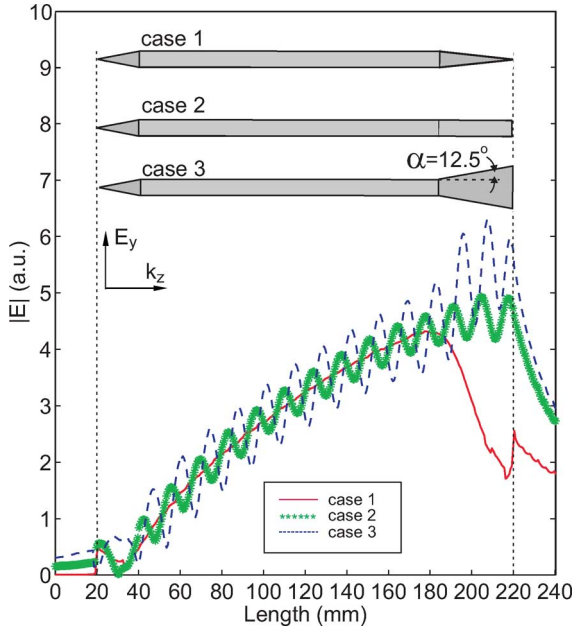

Fig. 2. Field distribution at the center of the dielectric rod along the axis for three different configurations.

It is mentioned in [6] that a feed taper and body taper are included after the waveguiding section in a typical dielectric rod antenna for an efficient transition from the exciting source, typically, a metallic waveguide and to suppresses side lobes, respectively. However, in the present scheme, the other end of the DFE was designed to have an E-plane flare similar to those described in [8]. This allows for control of the near field for near-field coupling to the DRA. A flare length of $1.25\lambda_0$ and flare angle of 12.5 degrees were chosen based on the desire to maximize achievable near-field strength for the given guide length and cross section acquired from step 1. The E-flared section provides an impedance mismatch between its face and free space where a reflected wave is generated in the rod. Fig. 2 shows three simulation results for the field distribution at the center of the dielectric rod along the axis. The various configurations for the end-section highlight the need for the E-flared section. We will compare case 1 with a tapered section, case 2 with a non-tapered section, and case 3 with a flared section. The simulations consist of a plane wave incident upon the terminal taper of the DFE. In case 1, the field amplitude of the guided propagating wave is seen to grow along the length of the guide due to the continuous coupling of the incident plane wave to the guide. The field amplitude then decays in the taper, where the guided wave is slowly impedance matched to free space. In case 2, a flare angle of 0 degrees is introduced and a resulting increase in the electric field at the face of the end-section is noted. The resulting field distribution in the guide shows a periodic variation along the length of the guide with a period of $\sim$12.75 mm ($\lambda_g/2$); λ_g is the guided wavelength for the TE_{11}^x mode in the guide where the propagation constant of $\beta_z = 246$ rads/m in the axis direction is obtained using Marcatili's method [9]. In case 3, a flare angle of 12.5 degrees is introduced. A similar periodic variation in the field distribution of the guided mode exists, while the electric field at the face of the end-section is higher than that of case 2. The increase in the electric field at the face for case 2 and 3 relative to case 1 is due to a mismatch between the face and free space, where a field distribution much like a standing wave is generated. Therefore, with a flare angle of 12.5 degrees, a strong field at the face can then be near-field coupled to the DRA. The final dimensions of the DFE are shown in Fig. 1(b). Traditionally, dielectric rod antennas are considered travelling wave antennas, however in this case, the DFE in such a configuration can certainly be considered unique in the sense that it is a travelling/standing wave hybrid structure.

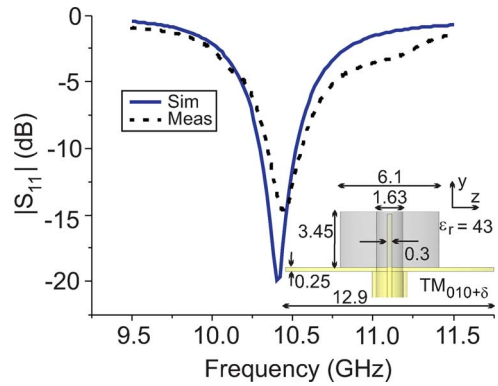

Fig. 3. $\mathrm{TM}_{010+\delta}$ mode monopole DRA reflection coefficient and its millimeter dimensions shown in the inset.

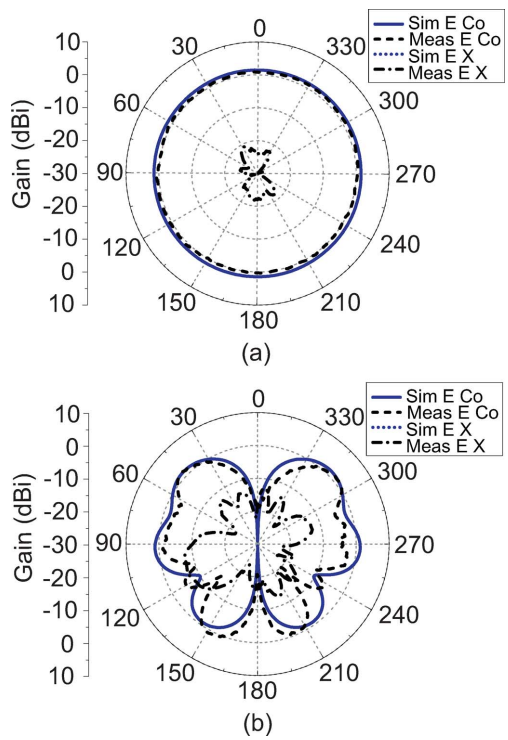

Fig. 4. $\mathrm{TM}_{010+\delta}$ mode monopole DRA (a) H-plane and (b) E-plane far-field gain patterns. Simulated cross polarization in both cases is extremely small.

III. Measurements and Discussions

An annular ring DRA operating in the electric monopole $\mathrm{TM}_{010+\delta}$ mode was fabricated [10], [11]. A ground plane for the annular ring DRA much smaller than a wavelength was selected so as to allow for close coupling between the annular ring DRA and DFE, which then leads to a radiation pattern that is not exactly that of an ideal monopole, as will be shown. Following this approach, an annular ring DRA, as shown in Fig. 3, with permittivity of 43, height of 3.45 mm ($0.12\lambda_0$), radius of 3.05 mm ($0.11\lambda_0$), center cutout radius of 0.815 mm ($0.03\lambda_0$), and ground plane radius of 6.45 mm ($0.22\lambda_0$) was designed and fabricated to verify the simulations. The designed resonant frequency was 10.35 GHz. After fabrication and measurements, it was found to have resonated at 10.45 GHz. With this information, the design for the DFE discussed in Section II was then made to center around 10.45 GHz. Fig. 3 shows the simulated and measured reflection coefficient for the electric monopole $\mathrm{TM}_{010+\delta}$ mode annular ring DRA, which was coaxially excited. The results are in close agreement, with

Fig. 5. Measurement setup of DFE coupling to the $\mathrm{TM}_{010+\delta}$ mode monopole DRA.

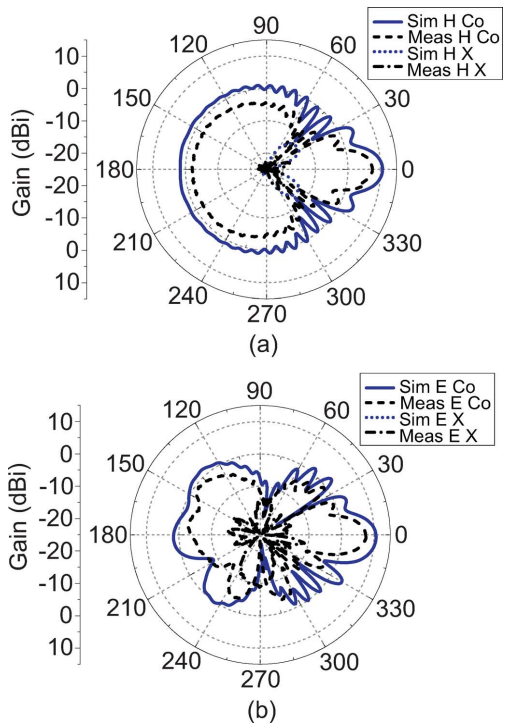

Fig. 6. $\mathrm{TM}_{010+\delta}$ mode monopole DRA and DFE combined (a) H-plane and (b) E-plane far-field gain patterns. Simulated cross polarization in both cases is extremely small.

only a 100 MHz, or 1% shift in frequency. The shift could be due to a small chip on the cylindrical DRA created during the machining process, some possible air gap between the DRA and the ground plane as mentioned in [12], [13], or a difference in the reported relative permittivity due to manufacturer tolerances. The H (xz plane) and E-plane (yz plane) radiation patterns of the DRA are illustrated in Fig. 4 and as expected, resemble those of a monopole, but with a noticeable amount of scalloping due to the finite ground plane. The simulated gain of the monopole DRA is 1.5 dBi and the maximum measured gain is 1.30 dBi. The slight difference in gain and radiation pattern is most likely due to the mentioned imperfections. However, the point of interest is the relative increase of the gain and its resulting radiation pattern after the inclusion of the DFE and hence this annular ring DRAs characteristics are adequate.

After verifying the annular ring DRA's performance, the DFE was then closely coupled, namely, 4 mm away. Fig. 5 illustrates the test setup with the annular ring DRA and the DFE, which is supported by a styrofoam stage. The results qualitatively followed the simulations. For example, at a 4 mm coupling distance, the measured gain is 9.07 dBi, giving a gain increase of 7.77 dB (compared to the measured gain of the monopole excited DRA alone). From simulations, at a 4 mm coupling distance, the gain with and without the DFE were 10.64 dBi and 1.5 dBi respectively. Therefore, a simulated difference of 9.14 dB was predicted. The difference between the simulated difference, 9.14 dB, and measured difference, 7.77 dB, could be attributed to a possible misalignment between the DRA and the DFE. The gain was found, in simulations, to be sensitive to the relative positioning (parallelism) of the annular ring DRA to the DFE. Additionally, the loss in the polystyrene may be higher than expected leading to a smaller increase in gain from the DFE.

To ensure a fair comparison, it is important to note that a decrease in power illuminating the antenna under test (the annular ring DRA, DFE combination) was made relative to the power level used for the annular ring DRA only system. Namely, the signal generator output level was decreased with the addition of the DFE to ensure that the plane wave incident on the DRA, DFE combination had the same power density as the case with only the annular ring DRA. Fig. 6 details the H (xz plane) and E-plane (yz plane) cuts. For both cuts, it is interesting to note that the radiation pattern is a hybrid of the directional pattern of the DFE and the pattern of the annular ring DRA. The half-power beamwidth (HPBW) in the H-plane is measured to be $\sim$18 degrees compared with the simulation of $\sim$19 degrees. The HPBW in the E-plane is measured to be $\sim$18 degrees compared with the simulation of $\sim$21 degrees. In both planes, the measured and simulated HPBWs are in close agreement with simulations.

IV. Conclusion

Through the use of numerical simulations and measurements, a DFE is shown to be an effective field enhancing passive element that can be used for radiation pattern modification and gain enhancement. An annular ring DRA was used to help characterize and verify the characteristics of the DFE. By characterizing the realized gain of the annular ring DRA before and after the addition of the DFE, it was concluded that the DFE changed the omnidirectional radiation pattern to that of a directional pattern. The directional field pattern was also found to have increased gain in the main lobe, which can be interpreted as a field enhancement within the DRA when illuminated by a plane wave in the same direction as the main lobe. The DFE demonstration here centered about the resonant frequency of the DRA, however, the DFE can potentially be used for applications with larger bandwidth requirements.

Although, the only mode discussed in this communication is a $\mathrm{TM}_{010+\delta}$ in the DRA, different mode profiles and DRA geometries could possibly be used. The coupling between the DFE and the DRA is primarily determined by the matching of the polarization between the DRA and the DFE. For example, if a $\mathrm{TE}_{010+\delta}$ mode cylindrical DRA is used, the DFE can efficiently couple to the DRA by rotating the DRA such that its electric field component is co-polarized to that of the DFE. With the above in mind, a variety of other non dielectric based antennas could be used as well.

References

[1] Z. Jiajie, W. Anguo, and W. Peng, "A survey on reconfigurable antennas," in *Proc. Int. Conf. on Microwave and Millimeter Wave Technology*, Apr. 2008, vol. 3, pp. 1156–1159.

[2] X.-S. Yang, B.-Z. Wang, and W. Wu, "Pattern reconfigurable patch antenna with two orthogonal quasi-Yagi arrays," in *Proc. IEEE, Antennas and Propagation Society Int. Symp.*, Jul. 2005, vol. 2B, pp. 617–620.

[3] N. Jin, F. Yang, and Y. Rahmat-Samii, "A novel patch antenna with switchable slot (PASS): Dual-frequency operation with reversed circular polarizations," *IEEE Trans. Antennas Propag.*, vol. 54, pp. 1031–1034, Mar. 2006.

[4] A. Ayazi, R. Hsu, B. Houshmand, and B. Jalali, "All-dielectric photonic assisted wireless receiver," in *Proc. 20th Annu. Meeting of the IEEE Lasers and Electro-Optics Society*, Oct. 2007, pp. 42–43.

[5] R. Hsu, A. Ayazi, B. Houshmand, and B. Jalali, "All-dielectric wireless receiver," in *Proc. IEEE/MTT-S Int. Microwave Symp.*, Jun. 2007, pp. 221–224.

[6] H. Jasik, *Antenna Engineering Handbook*. New York: McGraw-Hill, 1961.

[7] G. E. Mueller and W. A. Tyrrell, "Polyrod antennas," *Bell Syst. Tech. J.*, vol. 26, pp. 837–851, Oct. 1947.

[8] C. F. C. Salema and R. K. Jha, *Solid Dielectric Horn Antenna*. Norwood, MA: Artech House, 1998.

[9] E. Marcatili, "Dielectric rectangular wave guide and directional coupler for integrated optics," *Bell Syst. Tech. J.*, vol. 48, pp. 2071–2102, 1969.
[10] A. Petosa, *Dielectric Resonator Antenna Handbook*. Norwood, MA: Artech House, 2007.
[11] K. M. Luk and K. W. Leung, *Dielectric Resonator Antennas*. London, U.K.: Research Studies Press, 2003.
[12] G. Junker, A. Kishk, A. Glisson, and D. Kajfez, "Effect of fabrication imperfections for ground-plane-backed dielectric-resonator antennas," *IEEE, Antennas Propag. Mag.*, vol. 37, pp. 40–47, Feb. 1995.
[13] S. Shum and K. Luk, "Characteristics of dielectric ring resonator antenna with an air gap," *Electron. Lett.*, vol. 30, pp. 277–278, Feb. 1994.

Chipless RFID Tag Using Multiple Microstrip Open Stub Resonators

C. M. Nijas, R. Dinesh, U. Deepak, Abdul Rasheed, S. Mridula, K. Vasudevan, and P. Mohanan

***Abstract*—A novel compact RFID tag employing open stubs in a microstrip transmission line is proposed. The prototype of the tag is fabricated on a substrate of dielectric constant 4.4 and loss tangent 0.0018. The tag consists of microstrip open stub resonators and cross polarized transmitting and receiving disc monopole antennas. A prototype of 8 bit data encoded tag is demonstrated in this communication. Method for enhancing the performance of the RFID tag is also proposed. Magnitude or group delay response can be used to decode the tag informations.**

***Index Terms*—Chipless RFID tag, cross polarization, group delay, microstrip open stub, UWB antenna.**

I. Introduction

Radio frequency identification (RFID) can be conveniently employed to replace the barcode in the area of contactless data capturing. RFID doesn't require a face to face communication between data carrying device like transponder/RFID tag and interrogator/RFID reader. The RFID tag can be hidden inside the items and ensure more security and flexibility. The cost of the RFID tags with small chip is higher compared to barcode due to presence of application specific integrated circuit (ASIC) chip. Different RFID technologies are used for different applications. Some applications require short-range (up to 1.5 m) low-cost tags (luggage tagging), while others require long-range (over 20 m) and more reliable/robust tags (expensive equipment tagging or vehicle tagging).

RFID researchers are now focusing in the area of chipless RFID tags, in which bits are encoded in the frequency spectrum, and seem to be a promising solution for low-cost item tagging. Commercially available chipless RFID tags are developed by RFSAW and it is based on the surface acoustic waves (SAWs) [1]. These tags are not fully printable because of the piezoelectric components embedded in it. Fully printable chipless RFID based on group delay encoding [2], [3] and multi resonators [4] have been reported. Group delay based tag requires very large area for more number of bits. On the other hand, the power difference between the presence and absence of a bit is of the order of 1 dB in the case of multi resonator based RFID. This makes it very difficult for faithful identification.

A chipless RFID tag with microstrip open resonators and cross polarized disc monopole antennas is discussed in this communication. The proposed tag is very compact and can be easily decoded due to the large difference between reflected power level corresponding to the presence and absence of a bit. Compared to [2], [4], [5], this tag offers a difference of 5 dB in magnitude and 6 ns in group delay and hence can be easily decoded.

Manuscript received February 07, 2012; revised April 12, 2012; accepted May 04, 2012. Date of publication July 03, 2012; date of current version August 30, 2012. This work was supported in part by the Department of Science and Technology (DST), Government of India and University Grants Commission (UGC), Government of India.

C. M. Nijas, R. Dinesh, U. Deepak, A. Rasheed, K. Vasudevan and P. Mohanan are with the Centre for Research in ElectroMagnetics and Antennas (CREMA), Department of Electronics, Cochin University of Science and Technology, Cochin-22, Kerala, India (e-mail: drmohan@gmail.com).

S. Mridula is with the School of Engineering, Cochin University of Science and Technology, Cochin-22, Kerala, India.

Color versions of one or more of the figures in this communication are available online at http://ieeexplore.ieee.org.

Digital Object Identifier 10.1109/TAP.2012.2207081

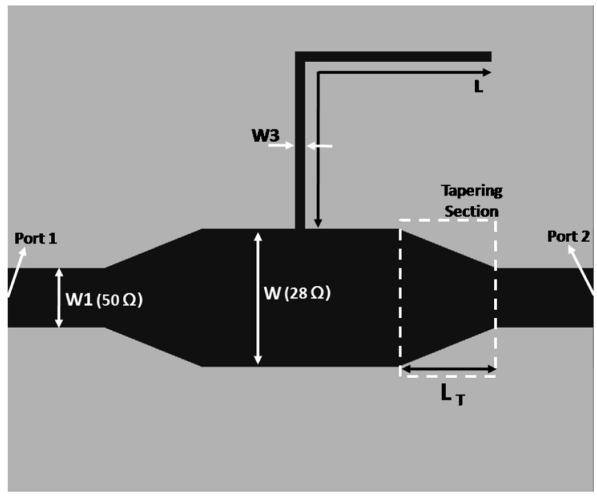

Fig. 1. Transmission line with quarter wave open stub resonator $W1 = 3\,\mathrm{mm}$, $W3 = 0.5\,\mathrm{mm}$, $W = 7\,\mathrm{mm}$ $L_T = 12\,\mathrm{mm}$ and $L = 18\,\mathrm{mm}$.

II. Tag Design

The evolution of tag from a simple transmission line is demonstrated here. A microstrip transmission line of 50 Ω is fabricated on a substrate of dielectric constant 4.4 and loss tangent 0.0018. A $\lambda_g/4$ open circuited stub with appropriate end correction [6] is connected at the centre of the transmission line, where λ_g is the guided wavelength at the operating frequency. The basic structure of the tag incorporating an open ended microstrip stub is shown in Fig. 1. It is noted that there is a band notch centred at 2.35 GHz when an open circuited stub of length 18 mm and width 0.5 mm is connected to the microstrip transmission line. This property of the stub is effectively utilized for the development of the tag. Simulation studies of a single stub microstrip transmission line for different line parameters using Ansoft HFSS are shown in Table I. From Table I.a it is found that when the transmission line impedance is 50 Ω ($W = 3\,\mathrm{mm}$), the system offers a fractional band width (FBW) of 30.05%. The FBW is estimated using, $\mathrm{FBW} = \Delta f/f_0 * 100\%$, where Δf is the 3 dB S21 band width and f_0 is the notch frequency. The aim is to reduce the FBW to get the narrowest possible resonance at the desired frequency. However, when the transmission line impedance is about 28 Ω ($W = 7\,\mathrm{mm}$), optimum FBW (12.57%) is achieved. It is noted that further decrease in the impedance of the transmission line distorts the S_{21} characteristics. So this impedance is selected for further analysis. From Table I.b it is again found that when the width of the $\lambda_g/4$ stub (W3) is decreasing,